Modeling solvent evaporation during thin film formation in phase separating polymer mixtures

John Cummings,[†] John S. Lowengrub,[‡] Bobby G. Sumpter,[¶,§] Steven M. Wise,[*,†] and Rajeev Kumar[*,†,¶,§]

[†]*Department of Mathematics, The University of Tennessee, Knoxville, TN-37996*

[‡]*Department of Mathematics, The University of California, Irvine, CA-92697*

[¶]*Computational Sciences and Engineering Division, Oak Ridge National Laboratory, Oak Ridge, TN-37831*

[§]*Center for Nanophase Materials Sciences, Oak Ridge National Laboratory, Oak Ridge, TN-37831*

E-mail: swise1@utk.edu; kumarr@ornl.gov

Abstract

Preparation of thin films by dissolving polymers in a common solvent followed by evaporation of the solvent has become a routine processing procedure. However, modeling of thin film formation in an evaporating solvent has been challenging due to a need to simulate processes at multiple length and time scales. In this work, we present a methodology based on the principles of linear non-equilibrium thermodynamics, which allows systematic study of various effects such as the changes in the solvent properties due to phase transformation from liquid to vapor and polymer thermodynamics resulting from such solvent transformations. The technique allows for the derivation of

evaporative flux and boundary conditions near each surface for simulations of systems close to the equilibrium. We apply it to study thin film microstructural evolution in phase segregating polymer blends dissolved in a common volatile solvent and deposited on a planar substrate. Effects of the evaporation rates, interactions of the polymers with the underlying substrate and concentration dependent mobilities on the kinetics of thin film formation are studied.

Introduction

Evaporation of liquid molecules[1–5] is ubiquitous in nature and used in a number of applications including coatings[6,7] and organic electronics.[8–11] Evaporation of liquids involves various transport phenomena in the linear[12–18] and nonlinear[19,20] regimes, which include momentum, heat and mass transfer. Also, evaporation of any liquid involves phase transformation from liquid to vapor, which becomes coupled with the transport phenomena. Modeling of evaporation must take into account the couplings between the kinetics of phase transformation and various transport phenomena in an accurate manner. The need for accurate models providing insights into evaporation for various phenomena occuring in nature and engineering cannot be overstated. Accurate models can help many engineering processes be more cost-effective and more efficient by providing fundamental understanding of various processes involved in the evaporation.

In 1997, Deegan et al.[21] reported a study on a drying sessile droplet containing solute and presented an explanation for the ring pattern observed in the dried state. This, so called coffee-ring effect, was explained[4,5,21–26] in terms of mass transfer of the solute and inhomogeneous evaporation rate, where the latter was shown to be the highest (in fact, divergent) near the pinned contact line separting liquid, vapor and solid. A number of reports focusing on various other effects due to hydrodynamics, depinning/motion of the contact line, temperature and gravitation have been reported in the literature.[25–35] Conclusions from a large number of studies focusing on evaporation in drops have been presented in a review

by Larson.[4] In particular, analytical relations for the inhomogeneneous evaporation rate, which varies radially for a spherical drop, have been derived using the lubrication approximation[1,4,22,23] (also called the long-wave theory[36,37]). The lubrication approximation leads to a set of equations where the original complexity of free-boundary problem get relaxed while preserving many important features of the underlying physics.[36,37] For example, in works by Clarke and co-workers[38,39] dealing with pattern formation in phase separating mixtures (without evaporation), the height of a film is treated using the lubrication approximation and can be coupled with diffusion of solutes in the film. A similar set of equations based on the lubrication approximation was derived by Thiele et al[37,40–42] and effects of solvent evaporation was considered. The coupled set of equations are called gradient dynamics description of thin films.[37,41] In recent works,[37] these equations were shown to be consistent with the Onsager's symmetry relations.[12–14] Differences in the works by Clarke and Thiele lie in the choice of conserved and non-conserved variables.[43] Use of the lubrication approximation allows explicit calculations for the evaporative flux,[4,21–26] which can be evaluated analytically for specialized shapes of the liquid-vapor interfaces such as in the case of spherical droplets with pinned contact lines.[21–23]

A number of other so-called moving boundary models[44–53] for *polymer* films, not relying on the lubrication approximation, have been developed and reported in the literature. Broadly, we can categorize these models into three classes. In the first class of models, local equilibrium near the liquid-vapor interface is assumed[44–48,51] and the evaporation is *assumed* to take place from the top of the liquid-vapor interface. Furthermore, the evaporative flux is taken to be proportional to the volume fraction of evaporating solvent at the top,[44–48,51] which results from the implicit assumption that the evaporative flux is diffusion limited.[44,45] Although this greatly simplifies the analytical[44–47] and numerical[48,51] treatment of solvent evaporation, details of the liquid-vapor interface can not be captured accurately using such models due to neglect of non-equilibrium nature of the liquid-vapor interfaces. These models are useful for providing morphological details far from the liquid-vapor interface. In the

second class of models, effects of solvent evaporation are simulated by simply removing the evaporating molecules at a given rate[49,53] and rescaling the volume fractions inside the simulation box. These models completely ignore principles of non-equilibrium thermodynamics. In the third class of models, liquid and vapor are allowed to be in non-equilibrium conditions. However, expressions of the evaporative fluxes are *assumed* e.g., the Hertz-Knudsen-Schrage relations are invoked,[50,52] rather than computed in a self-consistent manner using principles of non-equilibrium thermodynamics. Although these models provide useful insights into various processes resulting from the moving liquid-vapor interface leading to an increase in density inside the film, these models make simplified assumptions either about shape of the liquid-vapor interface or about the evaporative flux. Particle based simulations such as those based on the classical (Newtonian) molecular dynamics[54,55] have been used to obtain additional insights. However, in the case of processes occuring at widely disparate length and time scales (especially in the case of inhomogeneous polymeric systems), particle based simulations become computationally expensive and sometimes challenging to execute.

An accurate solvent evaporation model must account for the non-equilibrium nature of the liquid-vapor interfaces. This is evident from the Hertz-Knudsen-Schrage relations for the evaporative flux, which are based on the classical kinetic theory of gases.[56,57] In these relations, the evaporative flux depends on the temperature and pressure on both sides of the interface. However, usage of the Maxwell-Boltzmann distribution for the velocity of molecules in deriving these relations limit their range of validity and several empirical ways for interpretting experimental data for the evaporative fluxes have been devised.[57] Furthermore, there are cases when evaporative flux is not dominated by the diffusion of the vapors e.g., when evaporation takes place at very low pressure of the air. In these cases, the evaporative flux is affected by the rate of phase transformation from liquid to vapor and corresponds to faster evaporation in comparison with the diffusion dominated evaporation. Such cases have been explored extensively by Ward and co-workers[57–59] while studying evaporation of water and ethanol. A statistical rate theory based on the concept of transition probability

was used to derive an expression for the evaporative flux.[57,58] The theory accounts for thermally activated transfer of molecules from liquid to vapor phase and the thermal activation results from temperature differences between two sides of the liquid-vapor interfaces. The expression was used to estimate empirical coefficients,[57] which appear in the Hertz-Knudsen-Schrage relations for the evaporative flux. These works[57–59] have highlighted the importance of entropy production in the evaporation resulting from transfer of molecules from liquid to vapor phase due to discontinuities in temperature and pressure at the liquid-vapor interfaces. The entropy is generated near interfaces (also called interfacial entropy) due to the changes in the number of available quantum mechanical states resulting from transfer of molecules.[58,59] At equilibrium, the changes in entropy are zero and net rate of entropy production has been derived at the steady state.[59] As the entropy production is a central concept in the field of non-equlibrium thermodynamics, it is natural to develop a method for describing solvent evaporation using the ideas of non-equilibrium thermodynamics for systems close to equilibrium.[12–18] Constraint of near-equilibrium conditions can be realized in experiments, for example, when solvent evaporation is mainly used as a tool for overcoming the free energy barriers to reach the global free energy minimum state characterizing equilibrium. Solvent annealing for block copolymers[7] is an example.

Taking into account the entropy generation near equilibrium, we have developed a methodology to study solvent evaporation in multicomponent systems based on the concepts of linear non-equilibrium thermodynamics.[12–18] The methodology is limited to systems close to equilibrium. However, it is quite general and allows systematic investigations of various non-trivial effects. Vapors are included as an additional component in the theoretical description and expressions for the evaporative flux as well as boundary conditions are derived by making sure that in the long-time limit, the equilibrium state having the lowest free energy is obtained. Our approach is general enough to capture effects of diffusion, convection and phase transformation (or reaction) from liquid to vapor. Furthermore, the methodology makes it possible to simulate structure and dynamics of the liquid-vapor interface in

a self-consitent manner rather than assuming a flat interface allowing modeling of rough polymer-air interfaces.

Model Overview

We present a methodology for constructing a thermodynamically consistent model in order to study kinetics of thin film formation in a multi-component system in which one of the components is evaporating. As an example, we present the derivation for a quaternary system, which consists of two phase segregating polymers, liquid solvent and its vapors such that the solvent is volatile and evaporating. Generalization to other systems is straightforward. Construction of a model is based on the concept that near equilibrium, the total energy must be dissipated with time and approach a minimum free energy state representing an equilibrium in the limit of long time.

The rate of dissipation of the energy can be cast in the form of a variational principle [12–18] by constructing a function called the Rayleighian, which captures details of various dissipative processes. As per the variational principle, the rate of dissipation of the energy is the negative of a so-called, dissipation function. [12–14] This approach based on the dissipation function can be used to study couplings among mass, momentum and energy while considering conserved and nonconserved quantities. As an example, consider the so-called model-H, which considers coupling between thermal diffusion and hydrodynamics i.e., coupling between mass and momentum. [43] The standard model-H and its extended version for the study of moving "external" surfaces can be derived using the variational principle, which allows study of viscous and conentration dependent stresses (also called Korteweg stresses). [60] However, the functional form for the dissipation function is assumed to be known in order to use the variational principle and there is no prescription for deriving it. In this paper, we derive a functional form for the dissipation function by making sure that the rate of the dissipation of the total energy is maximum, which leads to a model similar to the model-H. As a *posteriori*

analysis, it is shown that an approach based on the Rayleighian with the derived functional form for the dissipation function leads to an identical set of equations (see the Supporting Information (SI)). In particular, for the quaternary polymer-polymer-liquid-vapor mixture, a set of three coupled Cahn-Hilliard[61] type equations along with a Poisson-like equation for the pressure is derived. Boundary conditions at different interfaces are systematically derived by making sure that they do not violate the concept of the dissipation even when the solvent vapors are allowed to exit from one of the computational boundaries.

Mass Conservation and Local Incompressibility Constraint

For a mixture of two polymers (p and q) and solvent (see Fig. 1), which can be present in the liquid phase (sl) or in the vapor phase (sv), we enforce the conservation of mass for each component through the continuity equations

$$\dot{\rho}_i(\boldsymbol{x},t) + \nabla\cdot(\rho_i(\boldsymbol{x},t)\boldsymbol{u}_i(\boldsymbol{x},t)) = S_i(\boldsymbol{x},t), \tag{1}$$

where $i \in \{\mathrm{p},\mathrm{q},\mathrm{sl},\mathrm{sv}\}$ and $\dot{\rho}_i(\boldsymbol{x},t) = \frac{\partial\rho_i(\boldsymbol{x},t)}{\partial t}$. The fields $\rho_i(\boldsymbol{x},t)$ and $\boldsymbol{u}_i(\boldsymbol{x},t)$ are the number density and velocity of the i^{th} component, respectively, at location $\boldsymbol{x}$ at time t. $S_i(\boldsymbol{x},t)$ is a source (or the reaction rate) term, which allows molecules to undergo phase change from the liquid to the vapor phase, for example, and is vital for modeling the evaporation of the volatile molecules. For the quaternary mixture with the evaporating solvent, $S_i(\boldsymbol{x},t) = 0$ for all $i \notin \{\mathrm{sl},\mathrm{sv}\}$. Introducing the volume fraction of the i^{th} component via the relation, $\phi_i(\boldsymbol{x},t) = \frac{\rho_i(\boldsymbol{x},t)}{\mathring{\rho}_i}$ – where $\mathring{\rho}_i > 0$ is the (constant) number density of the pure i^{th} phase at a fixed temperature T – we can rewrite Eq. (1) as

$$\dot{\phi}_i(\boldsymbol{x},t) + \nabla\cdot(\phi_i(\boldsymbol{x},t)\boldsymbol{u}_i(\boldsymbol{x},t)) = \mathring{\rho}_i^{-1} S_i(\boldsymbol{x},t). \tag{2}$$

Assuming that there are no voids in the mixture, so that

$$\sum_i \phi_i(\boldsymbol{x}, t) \equiv 1, \tag{3}$$

one of the volume fractions can be algebraically eliminated in terms of the others.

For the quaternary mixture with evaporating solvent, the liquid and the vapor phases of the solvent are distinct from each other only in terms of their respective number densities. We do not consider effects of thermal gradients in this work but these effects can be systematically included in the methodology presented here along the lines of Refs.[15,58,60,62,63] The source terms can lead to a change in the number of solvent molecules in an individual phase. In particular, we assume that

$$S_{\mathrm{sv}}(\boldsymbol{x}, t) = -S_{\mathrm{sl}}(\boldsymbol{x}, t). \tag{4}$$

Using the no-voids assumption (3) and the source term conservation condition (4), and summing Eq. (2), we obtain the following quasi-incompressibility condition

$$\sum_i \nabla \cdot (\phi_i(\boldsymbol{x}, t)\boldsymbol{u}_i(\boldsymbol{x}, t)) = \left(\mathring{\rho}_{\mathrm{sl}}^{-1} - \mathring{\rho}_{\mathrm{sv}}^{-1}\right) S_{\mathrm{sl}}(\boldsymbol{x}, t). \tag{5}$$

To identify the constraints on the velocities at the boundaries (cf. Fig. 1), we consider the total number of particles in the domain Ω, denoted M, which is defined as

$$M(t) = \sum_i \int_\Omega \mathring{\rho}_i \phi_i(\boldsymbol{x}, t) d\boldsymbol{x}. \tag{6}$$

Using the divergence theorem, the time derivative of M may be expressed as

$$\begin{aligned} \frac{dM(t)}{dt} &= \int_\Omega \sum_i \mathring{\rho}_i \dot{\phi}_i(\boldsymbol{x}, t) d\boldsymbol{x} \\ &= -\int_\Gamma \mathring{\rho}_i \phi_i(\boldsymbol{x}, t)\, \boldsymbol{u}_i(\boldsymbol{x}, t) \cdot \boldsymbol{n}\, d\boldsymbol{\sigma} + \int_\Omega \left[S_{\mathrm{sv}}(\boldsymbol{x}, t) + S_{\mathrm{sl}}(\boldsymbol{x}, t)\right] d\boldsymbol{x}, \\ &= -\int_\Gamma \mathring{\rho}_i \phi_i(\boldsymbol{x}, t)\, \boldsymbol{u}_i(\boldsymbol{x}, t) \cdot \boldsymbol{n}\, d\boldsymbol{\sigma} \end{aligned} \tag{7}$$

where $\boldsymbol{n}$ is the outward-pointing unit normal on the boundary of Ω, which is denoted Γ in Fig. 1. When no-flow or periodic boundary conditions for $\boldsymbol{u}_i \cdot \boldsymbol{n}$ are imposed at the boundary Γ, the time derivative is zero, i.e., the total number of particles remains constant in time. However, for the moment, we leave open the possibility that particles may flux across the boundary, and we discuss the boundary conditions for $\boldsymbol{u}_i \cdot \boldsymbol{n}$ in the next section.

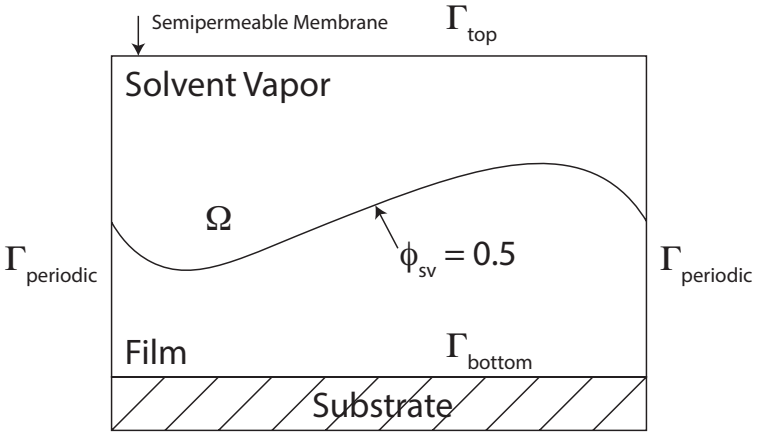

Figure 1: Schematic of the thin-film system considered in this work.

Thermodynamically Consistent Equations via the Principle of Maximal Energy Dissipation

In order to make further progress, we need constitutive equations relating the velocities and source terms to the volume fractions and thermodynamic quantities, such as the chemical potentials. We start by considering the free energy (F), written in a form, $F = F_b + F_s$ where

$$F_b = \int_\Omega f_b(\{\phi_i, \nabla\phi_i\}) d\boldsymbol{x}, \tag{8}$$

$$F_s = \int_\Gamma f_s(\{\phi_i\}) d\boldsymbol{\sigma} \tag{9}$$

so that f_b and f_s are the bulk and surface contributions to the free energy density, with functional dependencies on ϕ_i and its gradient. The quasi-incompressibility constraint in Eq. (5) is introduced in the time derivative of the free energy by using a Lagrange multiplier $p(\boldsymbol{x},t)$, so that

$$\sum_i \int_\Omega p(\boldsymbol{x},t)\nabla\cdot(\phi_i(\boldsymbol{x},t)\boldsymbol{u}_i(\boldsymbol{x},t))d\boldsymbol{x} = \int_\Omega p(\boldsymbol{x},t)\left(\mathring{\rho}_{\rm sl}^{-1}-\mathring{\rho}_{\rm sv}^{-1}\right)S_{\rm sl}(\boldsymbol{x},t)\,d\boldsymbol{x}. \tag{10}$$

The variable $p(\boldsymbol{x},t)$ will henceforth be referred to as the pressure. Taking the time derivative of the free energy functional and using Eq. 9, we have

$$\begin{aligned}\frac{dF}{dt} &= \sum_i \left\{ \int_\Omega \left\{ \mu_i(\boldsymbol{x},t)\dot{\phi}_i(\boldsymbol{x},t) + p(\boldsymbol{x},t)\left[\mathring{\rho}_i^{-1}S_i(\boldsymbol{x},t) - \nabla\cdot(\phi_i(\boldsymbol{x},t)\boldsymbol{u}_i(\boldsymbol{x},t))\right]\right\} d\boldsymbol{x} \right. \\ &\left. + \int_\Gamma \left[\frac{\partial f_s(\{\phi_i\})}{\partial\phi_i} + \sum_j \frac{\partial f_b}{\partial(\partial\phi_i/\partial x_j)} n_j \right] \dot{\phi}_i(\boldsymbol{x},t) d\boldsymbol{\sigma} \right\},\end{aligned} \tag{11}$$

where x_j and n_j are the $j^{\rm th}$ components of vectors $\boldsymbol{x}$ and $\boldsymbol{n}$, respectively, so that $\boldsymbol{x} = \{x_1, x_2, x_3\}$ and $\boldsymbol{n} = \{n_1, n_2, n_3\}$. Here, we have introduced the chemical potential of the $i^{\rm th}$ component, $\mu_i(\boldsymbol{x},t)$, defined as

$$\mu_i(\boldsymbol{x},t) = \frac{\delta F_b}{\delta\phi_i(\boldsymbol{x},t)} := \frac{\partial f_b}{\partial\phi_i} - \sum_j \frac{\partial}{\partial x_j}\frac{\partial f_b}{\partial(\partial\phi_i/\partial x_j)}, \tag{12}$$

i.e., the variational derivative of F_b with respect to ϕ_i. Now, using the continuity equation (2), Eq. (9) and the divergence theorem, we get

$$\begin{aligned}\frac{dF}{dt} = \sum_i \Bigg\{ & \int_\Omega \phi_i(\boldsymbol{x},t)\nabla\left[\mu_i(\boldsymbol{x},t) + p(\boldsymbol{x},t)\right]\cdot\boldsymbol{u}_i(\boldsymbol{x},t)\,d\boldsymbol{x} \\ & + \int_\Omega \left[\mu_i(\boldsymbol{x},t) + p(\boldsymbol{x},t)\right]\mathring{\rho}_i^{-1}S_i(\boldsymbol{x},t)d\boldsymbol{x} \\ & - \int_\Gamma \phi_i(\boldsymbol{x},t)\left[\mu_i(\boldsymbol{x},t) + p(\boldsymbol{x},t)\right]\boldsymbol{u}_i(\boldsymbol{x},t)\cdot\boldsymbol{n}\,d\boldsymbol{\sigma} \\ & + \int_\Gamma \left[\frac{\partial f_s(\{\phi_i\})}{\partial\phi_i} + \sum_j \frac{\partial f_b}{\partial(\partial\phi_i/\partial x_j)} n_j \right] \dot{\phi}_i(\boldsymbol{x},t) d\boldsymbol{\sigma} \Bigg\}.\end{aligned} \tag{13}$$

We assume that in the vicinity of the boundaries, the volume fractions equilibrate at a rate that is much faster than in the bulk. This is enforced by the "quasi-stationary" or "local thermodynamic equilibrium" boundary conditions

$$\frac{\partial f_s}{\partial \phi_i} - \frac{\partial f_s}{\partial \phi_{\mathrm{sv}}} + \sum_j \left[\frac{\partial f_b}{\partial(\partial \phi_i / \partial x_j)} - \frac{\partial f_b}{\partial(\partial \phi_{\mathrm{sv}} / \partial x_j)} \right] n_j = 0, \quad i \neq \mathrm{sv}. \tag{14}$$

Similar boundary conditions have been derived while considering surface contributions to the free energy of systems undergoing spinodal decomposition.[64,65] For the quaternary mixture, using Eqs. (4) and (13), Eq. (12) can be re-expressed as

$$\begin{aligned} \frac{dF}{dt} = & \sum_i \left\{ \int_\Omega \phi_i(\boldsymbol{x},t) \nabla \left(\mu_i(\boldsymbol{x},t) + p(\boldsymbol{x},t) \right) \cdot \boldsymbol{u}_i(\boldsymbol{x},t) d\boldsymbol{x} \right. \\ & \left. - \int_\Gamma \phi_i(\boldsymbol{x},t) \left(\mu_i(\boldsymbol{x},t) + p(\boldsymbol{x},t) \right) \, \boldsymbol{u}_i(\boldsymbol{x},t) \cdot \boldsymbol{n} \, d\boldsymbol{\sigma} \right\} \\ & + \int_\Omega \left(\mathring{\rho}_{\mathrm{sl}}^{-1} \mu_{\mathrm{sl}}(\boldsymbol{x},t) - \mathring{\rho}_{\mathrm{sv}}^{-1} \mu_{\mathrm{sv}}(\boldsymbol{x},t) + (\mathring{\rho}_{\mathrm{sl}}^{-1} - \mathring{\rho}_{\mathrm{sv}}^{-1}) p(\boldsymbol{x},t) \right) S_{\mathrm{sl}}(\boldsymbol{x},t) d\boldsymbol{x}. \end{aligned} \tag{15}$$

Now, linear constitutive relations for the velocities $\boldsymbol{u}_i(\boldsymbol{x},t)$, source $S_{sl}(\boldsymbol{x},t)$, and boundary velocity terms $\boldsymbol{u}_i(\boldsymbol{x},t) \cdot \boldsymbol{n}$ can be readily identified by (i) making sure that the equations result in a dissipation of the free energy and (ii) addressing the appropriate physical transport mechanisms associated to the microstructural evolution. Our first assumption is that the dynamics will be dominated by diffusion-like processes, and we neglect the effects of viscous flow. This suggests simple Darcy-type flow assumptions for the component velocities. Boundary flux of evaporating solvent is assumed to be non-zero, so that the total number of particles, M, can change in time. This is vitally important for evaporation processes in a fixed domain, since the vapor phase number density is significantly lower than that for the liquid phase. To summarize, we make the specific constitutive assumptions

$$\boldsymbol{u}_i(\boldsymbol{x},t) = -\gamma_i \phi_i(\boldsymbol{x},t) \nabla \left(\mu_i(\boldsymbol{x},t) + p(\boldsymbol{x},t) \right) \tag{16}$$

$$S_{\mathrm{sl}}(\boldsymbol{x},t) = -\lambda \left[\mathring{\rho}_{\mathrm{sl}}^{-1} \mu_{\mathrm{sl}}(\boldsymbol{x},t) - \mathring{\rho}_{\mathrm{sv}}^{-1} \mu_{\mathrm{sv}}(\boldsymbol{x},t) + (\mathring{\rho}_{\mathrm{sl}}^{-1} - \mathring{\rho}_{\mathrm{sv}}^{-1}) p(\boldsymbol{x},t) \right] \tag{17}$$

and

$$\boldsymbol{u}_i(\boldsymbol{x},t)\cdot\boldsymbol{n} = \begin{cases} \omega_i\phi_i(\boldsymbol{x},t)(\mu_i(\boldsymbol{x},t)+p(\boldsymbol{x},t)) \quad \text{on} \quad \Gamma_{\text{top}} \\ 0 \quad \text{on} \quad \Gamma_{\text{bottom}} \end{cases} \tag{18}$$

where γ_i, λ and ω_i are non-negative coefficients. Here, Γ_{top} and Γ_{bottom} represent the top and the bottom boundaries of the computational domain, respectively (Fig. 1). With these choices, we have

$$\begin{aligned} \frac{dF}{dt} = \sum_i \Bigg\{ &- \int_\Omega \gamma_i \left|\phi_i(\boldsymbol{x},t)\nabla\left(\mu_i(\boldsymbol{x},t)+p(\boldsymbol{x},t)\right)\right|^2 d\boldsymbol{x} \\ &- \int_{\Gamma_{\text{top}}} \omega_i \left[\phi_i(\boldsymbol{x},t)\left(\mu_i(\boldsymbol{x},t)+p(\boldsymbol{x},t)\right)\right]^2 d\boldsymbol{\sigma} \Bigg\} \\ &- \int_\Omega \lambda \left[\mathring{\rho}_{\text{sl}}^{-1}\mu_{\text{sl}}(\boldsymbol{x},t) - \mathring{\rho}_{\text{sv}}^{-1}\mu_{\text{sv}}(\boldsymbol{x},t) + (\mathring{\rho}_{\text{sl}}^{-1} - \mathring{\rho}_{\text{sv}}^{-1})p(\boldsymbol{x},t)\right]^2 d\boldsymbol{x} \leq 0. \end{aligned} \tag{19}$$

We observe that each process – diffusion, mass exchange, and boundary flux – independently dissipates the free energy. Our constitutive assumptions result in a dynamical system that represents a type of gradient flow, such that, up to the choices of the coefficients, the free energy decreases maximally, i.e., in the negative gradient direction. Of course, there are other constitutive choices that could lead to energy dissipation. For example, one could make assumptions such that one of the energy terms above had no definite sign, but proving energy dissipation would be challenging. Our theory is linear in the thermodynamic sense since the energy dissipation rates are quadratic, as can be observed in Eq. (18).

Eliminating the velocities and sources, we can write the governing equations purely in

terms of the functions ϕ_i, μ_i, and p as

$$\phi_{\rm sv}(\boldsymbol{x},t) = 1 - \sum_{i\neq {\rm sv}} \phi_i(\boldsymbol{x},t), \tag{20}$$

$$\begin{aligned}&\dot{\phi}_{\rm sl}(\boldsymbol{x},t) - \nabla\cdot\left(\gamma_{\rm sl}\phi_{\rm sl}^2(\boldsymbol{x},t)\nabla\left(\mu_{\rm sl}(\boldsymbol{x},t) + p(\boldsymbol{x},t)\right)\right), \\ &\quad = -\mathring{\rho}_{\rm sl}^{-1}\lambda\left(\mathring{\rho}_{\rm sl}^{-1}\mu_{\rm sl}(\boldsymbol{x},t) - \mathring{\rho}_{\rm sv}^{-1}\mu_{\rm sv}(\boldsymbol{x},t) + (\mathring{\rho}_{\rm sl}^{-1} - \mathring{\rho}_{\rm sv}^{-1})p(\boldsymbol{x},t)\right),\end{aligned} \tag{21}$$

$$\dot{\phi}_i(\boldsymbol{x},t) - \nabla\cdot\left(\gamma_i\phi_i^2(\boldsymbol{x},t)\nabla\left(\mu_i(\boldsymbol{x},t) + p(\boldsymbol{x},t)\right)\right) = 0, \quad i = {\rm p},\ {\rm q}. \tag{22}$$

$$\begin{aligned}&-\sum_i \nabla\cdot\left(\gamma_i\phi_i^2(\boldsymbol{x},t)\nabla\left(\mu_i(\boldsymbol{x},t) + p(\boldsymbol{x},t)\right)\right) \\ &\quad = -\left(\mathring{\rho}_{\rm sl}^{-1} - \mathring{\rho}_{\rm sv}^{-1}\right)\lambda\left[\mathring{\rho}_{\rm sl}^{-1}\mu_{\rm sl}(\boldsymbol{x},t) - \mathring{\rho}_{\rm sv}^{-1}\mu_{\rm sv}(\boldsymbol{x},t) + (\mathring{\rho}_{\rm sl}^{-1} - \mathring{\rho}_{\rm sv}^{-1})p(\boldsymbol{x},t)\right].\end{aligned} \tag{23}$$

The boundary conditions are the local thermodynamic equilibrium conditions Eq. (13) and the dissipative flux boundary conditions Eq. (17). Periodic boundary conditions are imposed on the right and left (vertical) boundaries, simulating a film of infinite extent in the in-plane direction (cf. Fig. 1).

Change of Variables and Reformulation

A change of variables simplifies the structure of the equations by eliminating the chemical potential $\mu_{\rm sv}$. It also will help to clarify the structure of the flux boundary conditions. Consider the following redefined pressure and chemical potentials:

$$\widetilde{p}(\boldsymbol{x},t) = \mu_{\rm sv}(\boldsymbol{x},t) + p(\boldsymbol{x},t) \quad \text{and} \quad \widetilde{\mu}_i(\boldsymbol{x},t) = \mu_i(\boldsymbol{x},t) - \mu_{\rm sv}(\boldsymbol{x},t) \quad \text{for} \quad i = {\rm p},\ {\rm q},\ {\rm sl}. \tag{24}$$

Let us also define the parameter

$$\nu_{\rm s} := \left(\mathring{\rho}_{\rm sl}^{-1} - \mathring{\rho}_{\rm sv}^{-1}\right) = \frac{\mathring{\rho}_{\rm sv} - \mathring{\rho}_{\rm sl}}{\mathring{\rho}_{\rm sl}\mathring{\rho}_{\rm sv}}, \tag{25}$$

which is clearly negative, since $\mathring{\rho}_{\rm sv} < \mathring{\rho}_{\rm sl}$. The source term can be rewritten in terms of the

new variables as

$$S_{\rm sl}(\boldsymbol{x},t) = -\lambda\left[\mathring{\rho}_{\rm sl}^{-1}\widetilde{\mu}_{\rm sl}(\boldsymbol{x},t) + \nu_{\rm s}\widetilde{p}(\boldsymbol{x},t)\right]. \tag{26}$$

In terms of the new variables, the dynamical equations are

$$\dot{\phi}_{\rm sl}(\boldsymbol{x},t) - \nabla\cdot\left(\gamma_{\rm sl}\phi_{\rm sl}^2(\boldsymbol{x},t)\nabla\left(\widetilde{\mu}_{\rm sl}(\boldsymbol{x},t) + \widetilde{p}(\boldsymbol{x},t)\right)\right) = -\lambda\mathring{\rho}_{\rm sl}^{-1}\left[\mathring{\rho}_{\rm sl}^{-1}\widetilde{\mu}_{\rm sl}(\boldsymbol{x},t) + \nu_{\rm s}\widetilde{p}(\boldsymbol{x},t)\right], \tag{27}$$

and

$$\dot{\phi}_i(\boldsymbol{x},t) - \nabla\cdot\left(\gamma_i\phi_i^2(\boldsymbol{x},t)\nabla\left(\widetilde{\mu}_i(\boldsymbol{x},t) + \widetilde{p}(\boldsymbol{x},t)\right)\right) = 0, \quad \text{for} \quad i = \text{p},\ \text{q}, \tag{28}$$

with the pressure Poisson equation

$$-\sum_i \nabla\cdot\left(\gamma_i\phi_i^2(\boldsymbol{x},t)\nabla\widetilde{p}(\boldsymbol{x},t)\right) - \sum_{i\neq\text{sv}}\nabla\cdot\left(\gamma_i\phi_i^2(\boldsymbol{x},t)\nabla\widetilde{\mu}_i(\boldsymbol{x},t)\right) = -\lambda\nu_{\rm s}\left[\mathring{\rho}_{\rm sl}^{-1}\widetilde{\mu}_{\rm sl}(\boldsymbol{x},t) + \nu_{\rm s}\widetilde{p}(\boldsymbol{x},t)\right]. \tag{29}$$

The flux boundary conditions for these variables transform as follows: at the top boundary, $\Gamma_{\rm top}$, we have (from Eqs. 15 and 17), setting $\beta_i := \frac{\omega_i}{\gamma_i}$,

$$\nabla\widetilde{p}(\boldsymbol{x},t)\cdot\boldsymbol{n} = -\beta_{\rm sv}\widetilde{p}(\boldsymbol{x},t) \tag{30}$$

$$\nabla\left(\widetilde{\mu}_i(\boldsymbol{x},t) + \widetilde{p}(\boldsymbol{x},t)\right)\cdot\boldsymbol{n} = -\beta_i\left(\widetilde{\mu}_i(\boldsymbol{x},t) + \widetilde{p}(\boldsymbol{x},t)\right), \quad i\neq\text{sv}, \tag{31}$$

and at the bottom boundary, $\Gamma_{\rm bottom}$, we have

$$\nabla\widetilde{p}(\boldsymbol{x},t)\cdot\boldsymbol{n} = 0 \tag{32}$$

$$\nabla\left(\widetilde{\mu}_i(\boldsymbol{x},t) + \widetilde{p}(\boldsymbol{x},t)\right)\cdot\boldsymbol{n} = 0, \quad i\neq\text{sv}. \tag{33}$$

At the top boundary, $\Gamma_{\rm top}$, if we imagine that there is a semi-permeable membrane that allows only solvent vapor out of the system, which is plausible, since the solvent molecules should be significantly smaller than the polymers then $\beta_{\rm sv} > 0$, but $\beta_i = 0$, $i \neq \text{sv}$. We can

then satisfy our dissipative boundary conditions simply as

$$\nabla\widetilde{p}(\boldsymbol{x},t)\cdot\boldsymbol{n}=-\beta_{\rm sv}\widetilde{p}(\boldsymbol{x},t),\quad \nabla\widetilde{\mu}_i(\boldsymbol{x},t)\cdot\boldsymbol{n}=-\nabla\widetilde{p}(\boldsymbol{x},t)\cdot\boldsymbol{n},\quad i\neq{\rm sv},\quad \text{on}\quad \Gamma_{\rm top}. \tag{34}$$

On the bottom boundary, the no-flux boundary conditions are even easier to satisfy:

$$\nabla\widetilde{p}(\boldsymbol{x},t)\cdot\boldsymbol{n}=0,\quad \nabla\widetilde{\mu}_i(\boldsymbol{x},t)\cdot\boldsymbol{n}=0,\quad i\neq{\rm sv},\quad \text{on}\quad \Gamma_{\rm bottom}. \tag{35}$$

Now, eliminating the volume fraction of the solvent in the vapor phase in the free energy densities, we define

$$\begin{aligned}\widetilde{f}_b\left(\{\phi_i,\nabla\phi_i\}_{i\neq{\rm sv}}\right) &:= \widetilde{f}_b(\phi_{\rm sl},\phi_{\rm p},\phi_{\rm q},\nabla\phi_{\rm sl},\nabla\phi_{\rm p},\nabla\phi_{\rm q})\\ &:= f_b(1-\sum_{i\neq{\rm sv}}\phi_i,\phi_{\rm sl},\phi_{\rm p},\phi_{\rm q},-\sum_{i\neq{\rm sv}}\nabla\phi_i,\nabla\phi_{\rm sl},\nabla\phi_{\rm p},\nabla\phi_{\rm q}).\end{aligned}$$

Then, using the chain rule, we have

$$\begin{aligned}\widetilde{\mu}_i(\boldsymbol{x},t) &= \frac{\delta F_b(\{\phi_i,\nabla\phi_i\})}{\delta\phi_i}-\frac{\delta F_b(\{\phi_i,\nabla\phi_i\})}{\delta\phi_{\rm sv}}\\ &= \frac{\partial f_b}{\partial\phi_i}-\frac{\partial f_b}{\partial\phi_{\rm sv}}-\left(\sum_j\frac{\partial}{\partial x_j}\frac{\partial f_b}{\partial(\partial\phi_i/\partial x_j)}-\sum_j\frac{\partial}{\partial x_j}\frac{\partial f_b}{\partial(\partial\phi_{\rm sv}/\partial x_j)}\right)\\ &= \frac{\partial\widetilde{f}_b}{\partial\phi_i}-\sum_j\frac{\partial}{\partial x_j}\frac{\partial\widetilde{f}_b}{\partial(\partial\phi_i/\partial x_j)},\quad i\neq{\rm sv}.\end{aligned} \tag{36}$$

Likewise, defining

$$\widetilde{f}_s\left(\{\phi_i\}_{i\neq{\rm sv}}\right):=\widetilde{f}_s(\phi_{\rm sl},\phi_{\rm p},\phi_{\rm q}):=f_s(1-\sum_{i\neq{\rm sv}}\phi_i,\phi_{\rm sl},\phi_{\rm p},\phi_{\rm q}), \tag{37}$$

the local thermodynamic equilibrium boundary conditions transform as

$$\frac{\partial\widetilde{f}_s}{\partial\phi_i}+\sum_j\left[\frac{\partial\widetilde{f}_b}{\partial(\partial\phi_i/\partial x_j)}\right]n_j=0,\quad i\neq{\rm sv}. \tag{38}$$

Phase Separating Polymer Mixtures: A Flory-Huggins-Cahn-Hilliard Description

For modeling solvent evaporation in thin films of phase separating polymer blends, we use the Cahn-Hilliard[61] functional form for the inhomogeneous free energy density along with surface interaction terms. In particular, we write

$$f_b(\{\phi_i, \nabla\phi_i\}) = f_h(\{\phi_i(\boldsymbol{x}, t)\}) + \sum_i \frac{\epsilon_i^2}{2} |\nabla\phi_i(\boldsymbol{x}, t)|^2, \tag{39}$$

where f_h is the so-called homogeneous free energy density, which is modeled as

$$f_h(\{\phi_i\}) = k_B T \left(\sum_i \frac{\mathring{\rho}_i}{N_i} \phi_i(\boldsymbol{x}, t) \ln(\phi_i(\boldsymbol{x}, t)) + \sum_{i \neq j} \chi_{ij} \phi_i(\boldsymbol{x}, t) \phi_j(\boldsymbol{x}, t) - c\phi_{\text{sv}}(\boldsymbol{x}, t) \right). \tag{40}$$

The parameter k_B is the Boltzmann constant; T is the absolute temperature; χ_{ij} are the interaction parameters between components i and j; and ϵ_i^2 are defined as[66]

$$\epsilon_i^2 = \frac{\mathring{\rho}_i b_i^2 k_B T}{18}, \tag{41}$$

where b_i is the Kuhn segment length of the polymer of type i.

For a homogeneous mixture without any vapor phase, Eq. (38) becomes the Flory-Huggins free energy density. A phase diagram for the Flory-Huggins free energy density can be readily constructed using standard techniques. For the quaternary system with volatile solvent, we expect the vapor phase to be energetically favorable. Such a thermodynamic preference for the vapor phase is encoded in the free energy density by the linear term $c\phi_{\text{sv}}$ in Eq. (39). Specifically, c can be chosen so that the vapor is the minimum energy phase. The effect of this term is readily seen in the free energy plots. (See Figures S1 and S2 in SI). However, we

remark that this term has no contribution to the free energy itself when $\phi_{\rm sv} = 0$ (i.e., when the mixture has no vapor phase component).

On the top boundary $\Gamma_{\rm top}$, we take $f_s(\{\phi\}) \equiv 0$, and there is, therefore, no energetic preference of any of the phases to be near the boundary. On the bottom boundary, $\Gamma_{\rm bottom}$, we suppose that f_s has a linear dependence on the polymer volume fractions, so that

$$f_s(\{\phi_i\}) = \left[\alpha_{\rm p}\phi_{\rm p}(\boldsymbol{x},t) + \alpha_{\rm q}\phi_{\rm q}(\boldsymbol{x},t)\right]. \tag{42}$$

With an appropriate choice of parameters, an energetic preference exists for one of the polymer phases to partially or completely wet the substrate to which the film is attached.[67]

With the particular form of f_s given in Eq. (41), the local equilibrium boundary conditions on $\Gamma_{\rm bottom}$ (cf. Eq. (37)) may be expressed as

$$\alpha_i + (\epsilon_i^2 + \epsilon_{\rm sv}^2)\nabla\phi_i(\boldsymbol{x},t)\cdot\boldsymbol{n} = 0 \quad \text{for} \quad i = {\rm p},\ {\rm q}, \tag{43}$$

$$\nabla\phi_{\rm sl}(\boldsymbol{x},t)\cdot\boldsymbol{n} = 0. \tag{44}$$

Eqs. (26) – (28) may be written in dimensionless form by choosing characteristic length and time scales. The characteristic length is determined by the radius of gyration, $R_g^{\rm p}$, of the longer polymer, taken to be p, without loss of generality, where $R_g^{\rm p} = \sqrt{N_{\rm p}/6}b_{\rm p}$. The time scale is set equal to the Rouse time of polymer p: $\tau = (R_g^{\rm p})^2 N_{\rm p}/(\gamma_{\rm p}k_BT\mathring{\rho}_{\rm p})$. Defining $\hat{\boldsymbol{x}} = \boldsymbol{x}/R_g^{\rm p}$ and $\hat{t} = t/\tau$, we can write Eqs. (26) – (28) as

$$\dot{\phi}_{\rm sl}(\hat{\boldsymbol{x}},\hat{t}) - \hat{\nabla}\cdot\left(\frac{\gamma_{\rm sl}N_{\rm p}\phi_{\rm sl}^2(\hat{\boldsymbol{x}},\hat{t})}{\gamma_{\rm p}\hat{\rho}_{\rm p}}\hat{\nabla}\left(\hat{\mu}_{\rm sl}(\hat{\boldsymbol{x}},\hat{t}) + \hat{p}(\hat{\boldsymbol{x}},\hat{t})\right)\right) = \hat{S}_{\rm sl}(\hat{\boldsymbol{x}},\hat{t}), \tag{45}$$

$$\dot{\phi}_i(\hat{\boldsymbol{x}},\hat{t}) - \hat{\nabla}\cdot\left(\frac{\gamma_i N_{\rm p}\phi_i^2(\hat{\boldsymbol{x}},\hat{t})}{\gamma_{\rm p}\hat{\rho}_{\rm p}}\hat{\nabla}\left(\hat{\mu}_i(\hat{\boldsymbol{x}},\hat{t}) + \hat{p}(\hat{\boldsymbol{x}},\hat{t})\right)\right) = 0 \quad \text{for} \quad i = {\rm p},\ {\rm q}, \tag{46}$$

where $\hat{\rho}_i = \frac{\mathring{\rho}_i}{\mathring{\rho}_{\rm sl}}$; $\hat{\mu}_i(\hat{\boldsymbol{x}},\hat{t}) = \widetilde{\mu}_i(\boldsymbol{x},t)/\mathring{\rho}_{\rm sl}k_BT$; $\hat{p}(\hat{\boldsymbol{x}},\hat{t}) = \widetilde{p}(\boldsymbol{x},t)/\mathring{\rho}_{\rm sl}k_BT$;

$$\hat{S}_{\rm sl} = -\hat{\lambda}\left(\hat{\mu}_{\rm sl}(\hat{\boldsymbol{x}},\hat{t}) + \hat{p}(\hat{\boldsymbol{x}},\hat{t}) - \hat{\rho}_{\rm sv}^{-1}\hat{p}(\hat{\boldsymbol{x}},\hat{t})\right); \tag{47}$$

and $\hat{\lambda} = \tau\lambda\mathring{\rho}_{\rm sl}k_BT$. The time and space derivatives are hereafter understood to be with respect to non-dimensional time and space, respectively.

For the free energy calculated using Eq. (38), the $i^{\rm th}$ chemical potential transforms as

$$\hat{\mu}_i(\hat{\boldsymbol{x}},\hat{t}) = \frac{\partial \hat{f}_h(\{\phi_i\}_{i\neq \rm sv})}{\partial \phi_i} - \hat{\epsilon}_i^2\hat{\Delta}\phi_i(\hat{\boldsymbol{x}},\hat{t}) - \sum_{j\neq \rm sv}\hat{\epsilon}_{\rm sv}^2\hat{\Delta}\phi_j(\hat{\boldsymbol{x}},\hat{t}), \quad i \neq \rm sv, \tag{48}$$

where $\hat{\epsilon}_i^2 = \frac{\hat{\rho}_i b_i^2}{18(R_g^{\rm p})^2}$ and

$$\hat{f}_h(\{\hat{\phi}_i\}_{i\neq \rm sv}) = \frac{f_h(1-\sum_{i\neq \rm sv}\phi_i, \phi_{\rm sl}, \phi_{\rm p}, \phi_{\rm q})}{\mathring{\rho}_{\rm sl}k_BT},$$

which can be written in terms of dimensionless parameters $\hat{\chi}_{ij} = \chi_{ij}/\mathring{\rho}_{\rm sl}$. Also, writing the boundary conditions in terms of dimensionless parameters leads to two new quantities: $\hat{\beta}_{\rm sv} = \beta_{\rm sv}R_g^{\rm p}$ and $\hat{\alpha}_i = \alpha_i/(\mathring{\rho}_{\rm sl}R_g^{\rm p}k_BT)$, $i = $ p and q.

Results

In the following, we present results obtained after numerically solving the equations presented in the previous section. For details of the numerical methods, see the SI. It is to be noted that the rate of phase change (i.e., the source term, $S_{\rm sl}$ given by Eq. (16)) is directly coupled to the chemical potential of the liquid and the vapor, which is in qualitative agreement with a general expression for the evaporative flux derived by Ward et al.[58] In the model developed here for the phase separating polymer blends, motion of the interface separating the polymer blend and the vapor phase depends on the parameters, $\hat{\beta}_{\rm sv}$ and $\hat{\lambda}$, both of which affect the evaporative flux through the top boundary. Physically, $\beta_{\rm sv} = \omega_{\rm sv}/\gamma_{\rm sv}$ is a ratio of the velocity of the vapors near the top boundary characterized by $\omega_{\rm sv}k_BT$ and its diffusion constant, $\gamma_{\rm sv}k_BT$. It is to be noted that $\beta_{\rm sv}$ has units of length inverse. λ controls the rate of conversion/phase change from the liquid to the vapor phase. First we show the effects of $\hat{\beta}_{\rm sv}$ and $\hat{\lambda}$ on the motion of the interface separating the vapor phase from the polymer

blends. Later, results for the simulations executed in two dimensional space are presented, focusing on the effects of concentration dependent diffusion constants and effects of interfacial interactions.

Simulations in one dimensional space

Presented in this section are simulations analyzing the dependence of the model on the parameters $\hat{\beta}_{\rm sv}$ and $\hat{\lambda}$. Each simulation was run on a computational domain of $\hat{x} \in [0, 100]$. For $\hat{x} < 75$, all simulations were initialized with $\phi_{\rm p} = 0.1 + {\rm rand}(\hat{x})$ where ${\rm rand}(\hat{x})$ is a random number between -0.1 and 0.1, $\phi_{\rm q} = 0.15$ and $\phi_{\rm sv} = 10^{-8}$, with $\phi_{\rm sl}$ initialized to satisfy the no voids constraint $\sum_i \phi_i = 1$. In order to model a polymer mixture, with the solvent in the vapor phase above it, we initialized $\phi_{\rm sl} = \phi_{\rm p} = \phi_{\rm q} = 10^{-8}$, with $\phi_{\rm sv} = 1.0 - 3 \times 10^{-8}$ for $\hat{x} > 75$. By definition, $\hat{\rho}_{\rm sl} = 1.0$ and without any loss of generality, $\gamma_{\rm p} = 1.0$ can be chosen. For the sake of completeness, all of the parameters for running these simulations are presented in Table 1. All simulations were done on a grid with 128 spatial grid points and time step $\Delta\hat{t} = 0.001$. Typical plots of the vapor phase volume fraction ($\phi_{\rm sv}$) are presented in Fig. 2. Similar plots were obtained by varying $\hat{\beta}_{\rm sv}$ and $\hat{\lambda}$. The general qualitative behavior shown in Fig. 2 is expected for a mixture with an evaporating solvent. Initially, there was a vapor phase indicated by $\phi_{\rm sv} \approx 1$ on top of the polymer mixture containing $\phi_{\rm sv} \approx 0$. As the solvent in the liquid phase evaporated, the vapor phase grew until the solvent in the liquid phase completely ran out, after which the vapor phase cannot grow anymore.

Dependence of interface velocity on the parameters

Effects of the parameters, $\hat{\beta}_{\rm sv}$ and $\hat{\lambda}$, on the location of the interface between the polymer blend and the vapor phase are shown in Figs. 3 and 4, respectively. All of the other parameters are the same as in Table 1. The interface location is defined here to be the $\hat{x}$ such that $\phi_{\rm sv}(\hat{x}) = 0.5$ (which is unique in these simulations). Increasing the parameter $\hat{\beta}_{\rm sv} = \beta_{\rm sv} R_g^{\rm p}$, where $\beta_{\rm sv} = \omega_{\rm sv}/\gamma_{\rm sv}$, corresponds to varying $\omega_{\rm sv}$ for fixed $\gamma_{\rm sv}$, which increases

Table 1: Parameters for generating results shown in Fig. 2

Gradient Energy Coefficients		Mobilities		Densities	
$\hat{\epsilon}^2_{\rm sv}$	1.00	$\gamma_{\rm sv}$	5.0	$\mathring{\rho}_{\rm sv}$	0.010
$\hat{\epsilon}^2_{\rm sl}$	1.00	$\gamma_{\rm sl}$	5.0	$\mathring{\rho}_{\rm sl}$	1.0
$\hat{\epsilon}^2_{\rm p}$	1.00	$\gamma_{\rm p}$	1.0	$\mathring{\rho}_{\rm p}$	1.0
$\hat{\epsilon}^2_{\rm q}$	1.00	$\gamma_{\rm q}$	1.0	$\mathring{\rho}_{\rm q}$	1.0

Interaction Parameters	
$\hat{\chi}_{\rm sv,sl}$	1.7
$\hat{\chi}_{\rm sv,p}$	1.7
$\hat{\chi}_{\rm sv,q}$	1.7
$\hat{\chi}_{\rm sl,p}$	0.4
$\hat{\chi}_{\rm sl,q}$	0.9
$\hat{\chi}_{\rm p,q}$	1.0

Miscellaneous Parameters	
$\hat{\beta}_{\rm sv}$	1.000
$\hat{\lambda}$	0.001
$c/\mathring{\rho}_{\rm sl}$	5.0
$N_{\rm p}$	89.0
$N_{\rm q}$	7.0

the flux of vapor particles across the interface. Increasing $\hat{\lambda}$ increases the rate at which solvent particles in the liquid phase transition to solvent particles in the vapor phase. It is to be noted that these simulations were executed with the no flux boundary conditions on $\boldsymbol{u}_{\rm sl}$ so that solvent in the liquid form cannot directly flux in and out of the top boundary, but instead must transition first into vapor phase and then flux out in the vapor phase. These simulations were run with 256 spatial grid points on the domain $x \in [0, 100]$ with a time step of $\Delta\hat{t} = 0.001$. Both of the figures reveal that increase in either $\hat{\beta}_{\rm sv}$ or $\hat{\lambda}$ leads to faster motion of the interface, as expected. Although the one dimensional simulation runs provide information about the motion of the moving interface, these simulations do not provide any information about the mesoscale structure that can form during the solvent evaporation. In order to get information about the morphologies that can appear during the solvent evaporation, we have solved the set of equations in two dimensional space and results are presented below.

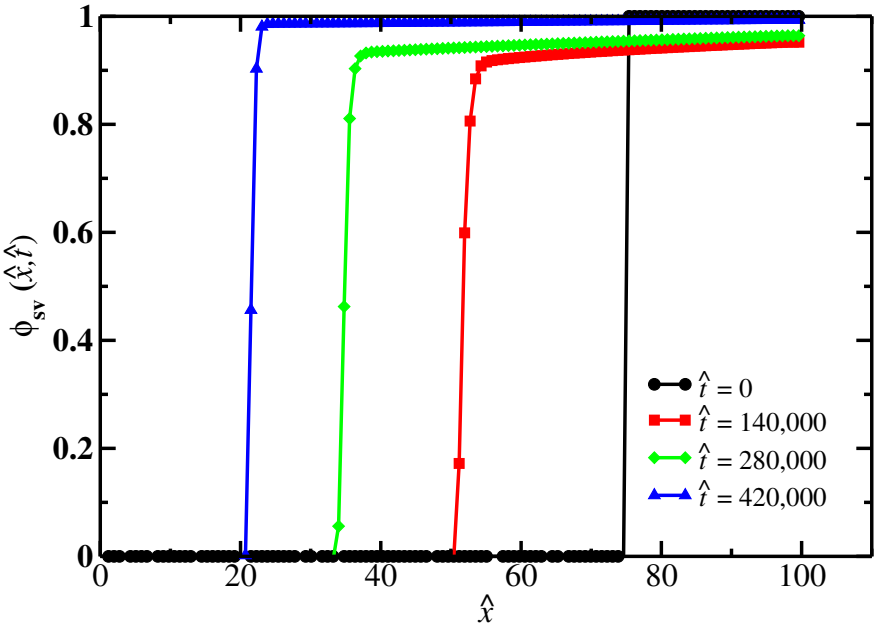

Figure 2: In this figure, we plot ϕ_{sv} at multiple time steps, and we use parameters from Table 1. It is shown that there is a well-defined interface between the vapor phase ($\phi_{\text{sv}} \approx 1$) and the polymer mixture ($\phi_{\text{sv}} \approx 0$), and that the polymer mixture shrinks in height until the solvent in the liquid phase has fully evaporated.

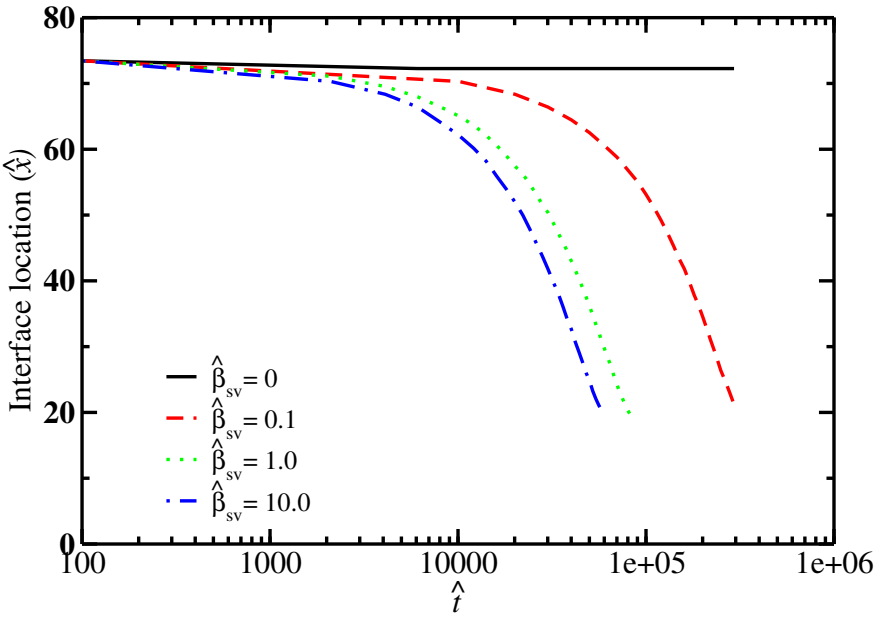

Figure 3: Dependence of location of the vapor-polymer interface on $\hat{\beta}_{\text{sv}}$ while $\hat{\lambda}$ is kept fixed at $\hat{\lambda} = 10^{-4}$.

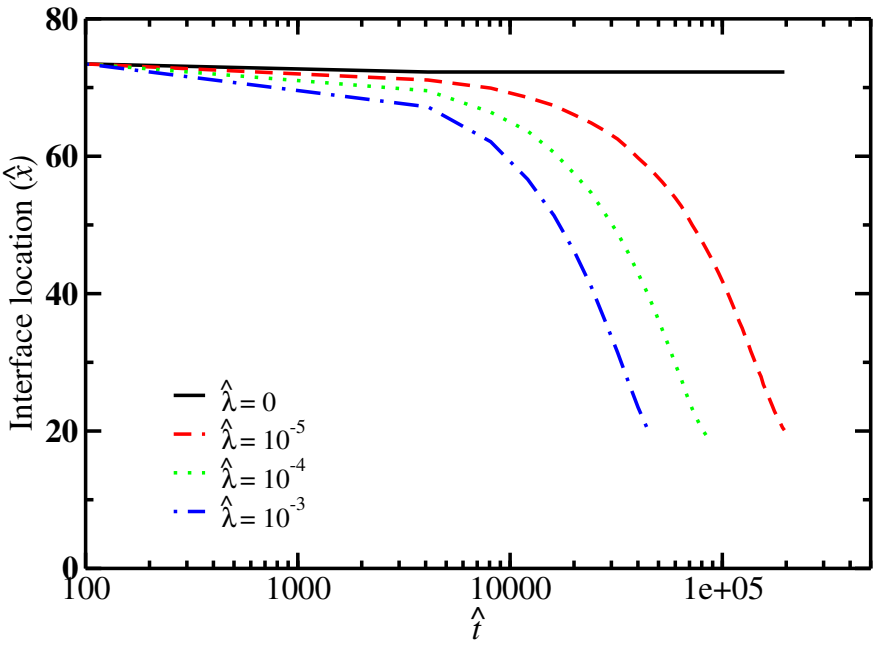

Figure 4: Dependence of location of the vapor-polymer interface on $\hat{\lambda}$ while $\hat{\beta}_{\mathrm{sv}}$ is kept fixed at $\hat{\beta}_{\mathrm{sv}} = 1$.

Simulations in two dimensional space

Simulations run in two dimensional space were used to understand the effects of different parameters of the model on the morphologies that can appear in thin films. For such purposes, we varied the coefficients of the square gradient terms as well as the diffusion constants parameterized by γ_i in the model. Furthermore, effects of preferential interactions with the substrates were studied by varying the coefficients of the surface energy terms, as described earlier. In each simulation, interaction parameters $\hat{\chi}_{\mathrm{sv,i}}$ was chosen to be large enough so that mixing of the solvent in the vapor phase with other components become highly energetically unfavorable. The other interaction parameters were chosen so that solvent in the liquid form prefers polymer p or q, and that polymer p and q are prone to demixing. Plots of either polymer p or q are provided, along with a red line indicating the interface between the polymer blend and the solvent in the vapor phase. Unlike the simulations executed in one dimensional space with no flux boundary conditions for $\boldsymbol{u}_{\mathrm{sl}}$, here we used finite flux boundary condition for the solvent in the liquid phase (sl) at the top boundary. In

particular, we used $\hat{\beta}_{sl} = \hat{\beta}_{sv} = 1.0, \hat{\beta}_{p} = \hat{\beta}_{q} = 0.0$. All simulations were done on a block structured adaptive mesh with the finest resolution at 128 spatial grid points in both the parallel (taken to be along y axis) and normal (taken to be along x axis) to the bottom boundary along with a temporal step of $\Delta\hat{t} = 10^{-4}$ using a semi-implicit method (see the SI for the details of the numerical algorithm). Initialization of the volume fractions were, for $\hat{x} < 75$ $\phi_{p}(\hat{x}, \hat{y}) = 0.1 + \text{rand}(\hat{x}, \hat{y})$ where $\text{rand}(\hat{x}, \hat{y})$ is a random number between -0.1 and 0.1, $\phi_{q}(\hat{x}, \hat{y}) = 0.15$, $\phi_{sv}(\hat{x}, \hat{y}) = 10^{-8}$, and $\phi_{sl}(\hat{x}, \hat{y})$ satisfying the no voids constraint. For $\hat{x} > 75$ (the initial vapor phase), we have $\phi_{sl}(\hat{x}, \hat{y}) = \phi_{q}(\hat{x}, \hat{y}) = \phi_{p}(\hat{x}, \hat{y}) = 10^{-8}$ with $\phi_{sv}(\hat{x}, \hat{y}) \approx 1$ satisfying the no voids constraint.

Effects of preferential interactions with a substrate

In order to understand the effects of preferential interactions with the underlying substrate, we have included surface energy contributions in the free energy with $\hat{\alpha}_{p} = -0.02$ and $\hat{\alpha}_{q} = 0.02$. Such a choice leads to a slight preference of the polymer p to be at the bottom boundary. All the other parameters are the same as in Table 1 with the exception of $\gamma_{sv} = \gamma_{sl} = 1.0$. Snapshots of ϕ_{p} at different time steps are shown in Fig. 5. In these simulations, the solvent in the liquid phase is being depleted near the interface of the polymer blend and the solvent in the vapor phase. As a result, concentration of the polymers p and q increases in the thin film (see Fig. 5(b) and (c)). Since $\hat{\chi}_{p,q}$ is large enough, it is energetically more favorable for polymers p and q to phase separate at higher concentrations. In the long time limit, the solvent gets completely removed so that $\phi_{sl} \approx 0$, and the final structure that is formed are pillar-like pure phases of the two polymers. Effects of the surface energy terms can be seen with the formation of non-perpendicular contact angles at the final time $\hat{t} = 27000$ in Fig. 5(d).

Final stratified or pillar like structures obtained in these simulations are found to be more stable than a homogeneous phase. These results are in qualitative agreement with studies focusing on the relative stability of pillar like structures with respect to the homogeneous

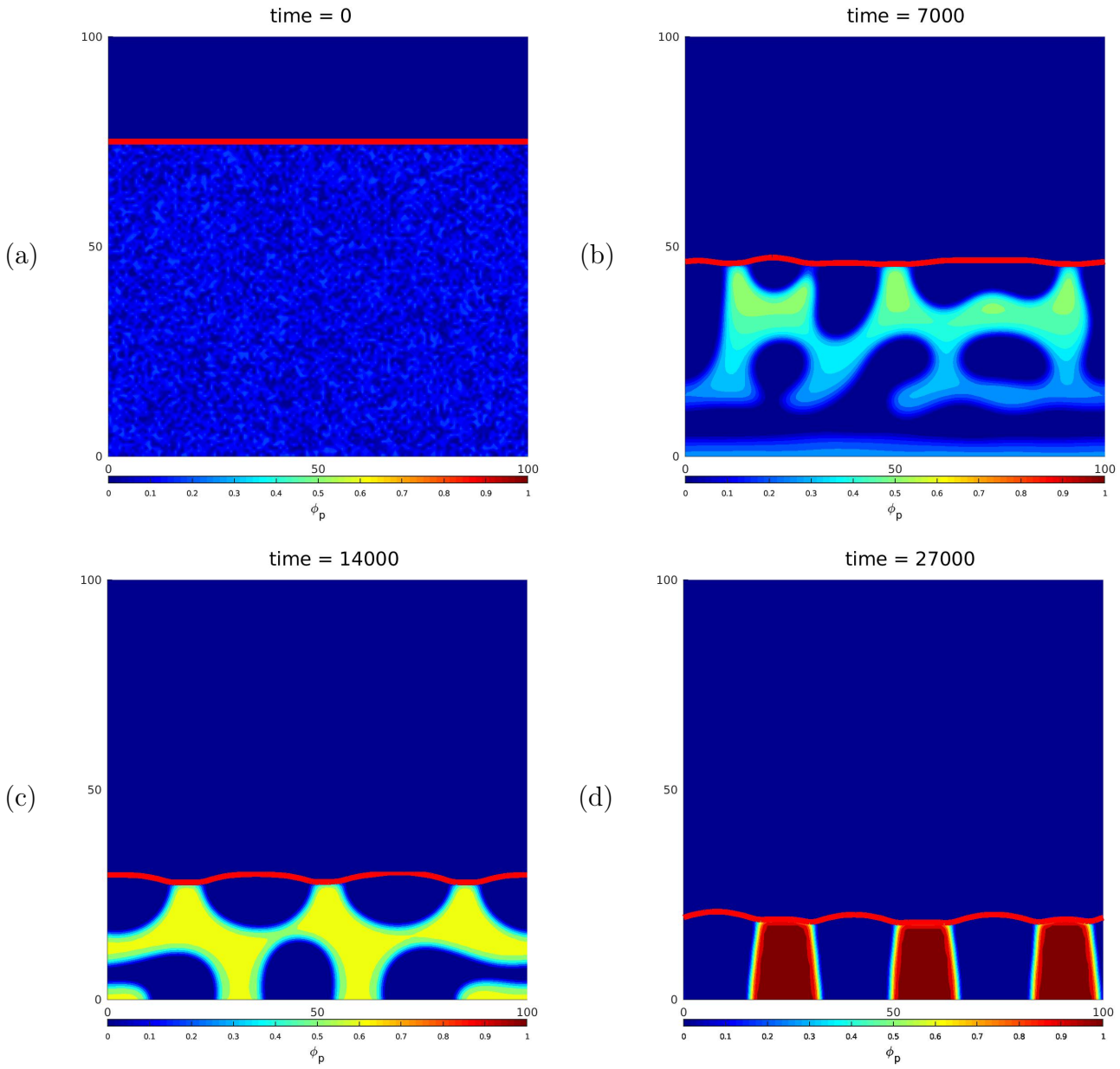

Figure 5: Effects of the surface energy terms on the phase separation in thin films containing evaporating solvent are shown here. (a) Initial configuration for $\phi_p = 0.1$, with random fluctuations as described in the main text. The red line indicate the interface between the mixture and the solvent in the vapor phase. (b) Phase separation as well as shrinkage of the thin film can be seen in this panel showing ϕ_p. (c) and (d) Effects of the surface energy terms can be seen with the formation of non-perpendicular contact angles at the final time $\hat{t} = 27000$.

films, although studied in the absence of solvent evaporation. These studies either used extended model-H[68,69] or constructed appropriate energy functional whose optimization leads to the time independent solution of the equations describing kinetics of phase separation in binary mixtures[70] in the steady state.

Effects of the square gradient coefficients

For understanding the effects of the coefficients, $\hat{\epsilon}_i^2$, we performed another simulation in which we doubled each $\hat{\epsilon}_i^2$ and kept all the other parameters the same as those used to obtain Fig. 5. This, in turn, means that spatial gradients of the volume fractions become energetically more unfavorable leading to lesser number of interfaces that can form (cf. Fig. 6). Furthermore, surface energy terms with $\hat{\alpha}_{\rm p} = -0.04, \hat{\alpha}_{\rm q} = 0.04$ were used to introduce the effects of the preferential interactions with the bottom substrate.

Effects of kinetic freezing

In the results discussed so far, stratified or pillar like structures were found to be stable with a smooth interface between the polymeric film and the vapor phase. Smooth polymer-air interfaces result from the fact that the mobility coefficients ,γ_i, were chosen to be independent of concentration. Physically, this is similar to the case of non-glassy polymers dissolved in a volatile solvent as discussed by de Gennes.[44] Another scenario of solvent evaporation in thin films containing glassy polymers was also treated by de Gennes[45] while discussing rough polymer-air interfaces and the origin of the roughness was attributed to the polymer rich "crust" build up near the air interface. A simple model for the crux formation (also called the skin formation) based on diffusive processes was devised by Doi and co-workers[46,47] where a cooperative diffusion constant was assumed to be concentation dependent.

Solvent evaporation in thin films containing glassy polymers can be treated using the current methodology by treating the coefficients, γ_i as concentration dependent so that mobility of polymers decrease with an increase in the volume fraction of the polymer due

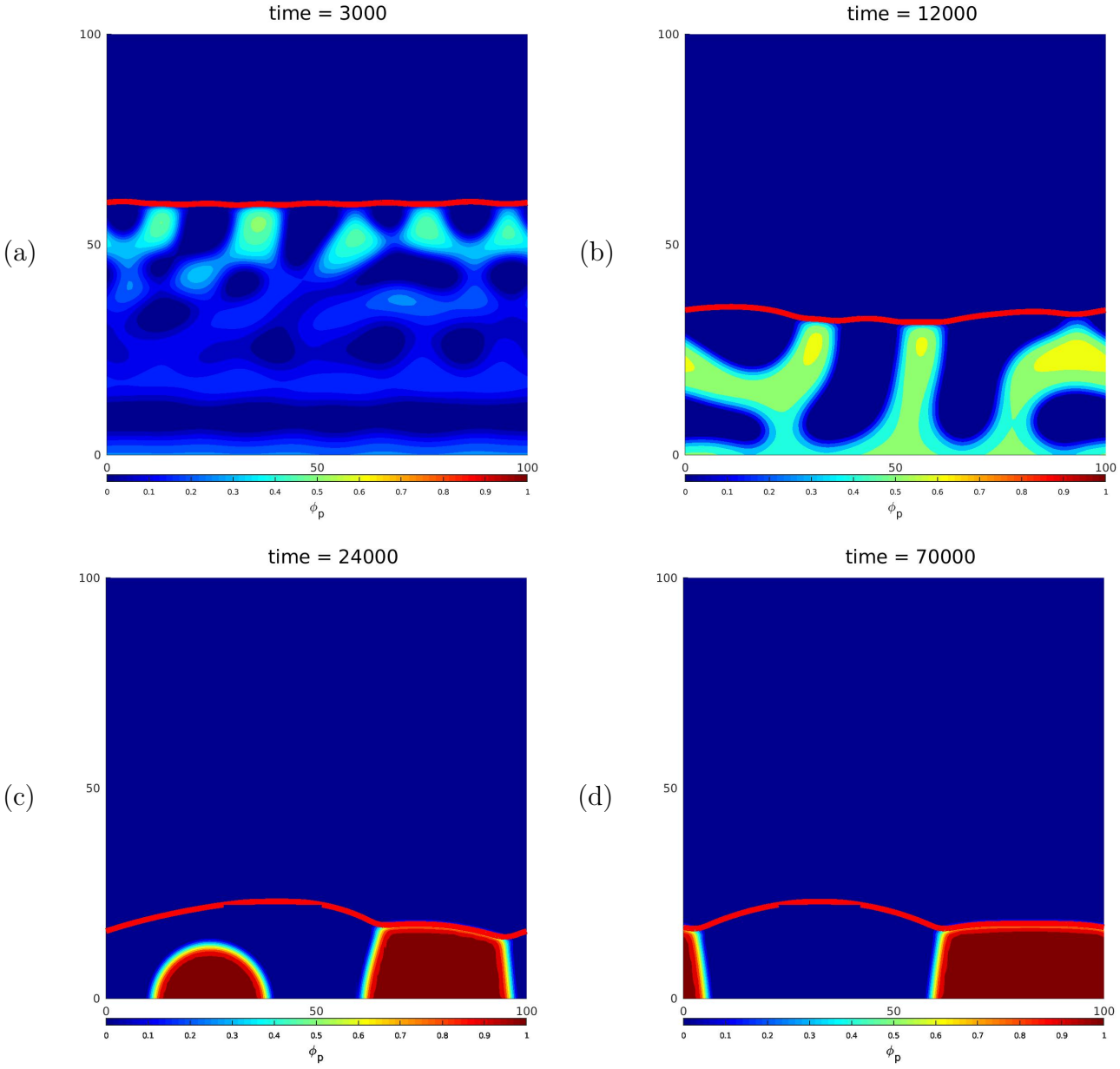

Figure 6: Effects of the square gradient coefficients, $\hat{\epsilon}_i^2$ on the morphology depicted via ϕ_p. We initialized $\phi_p = 0.1$ with random fluctuations throughout the simulation. (a)-(b) We see similar behavior to Fig. 5, with the polymer phase separating more near the vapor-polymer interface as the solvent in the liquid phase begins to transition out of the system. (c) As the solvent almost completely exits so that polymer rich phases are left, we see regions of pure polymer p ($\phi_p \approx 1$). (d) Long after the solvent has left the film, we see the last bubble of polymer ϕ_p diffuse into the larger region where $\phi_p \approx 1$. Though the end structure is similar to that of Fig. 5, we only see one pillar of each type of polymer appearing due to the fact that gradient energy terms $\hat{\epsilon}_i^2$ are twice as large in this simulation as opposed to the previous.

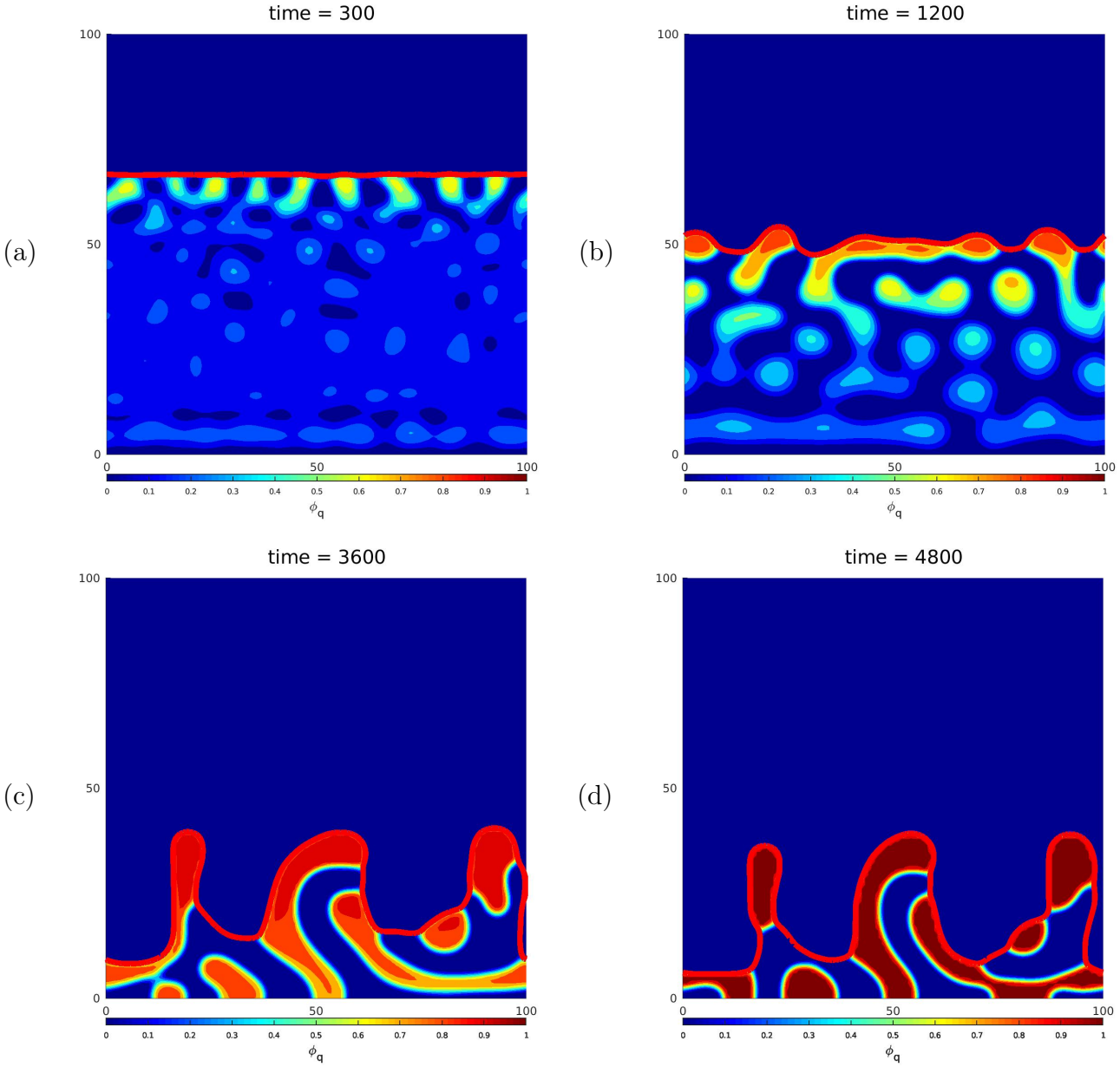

Figure 7: Effects of the concentration dependent γ_i on the structure in the thin films shown in terms of ϕ_q. (a) We see similar behavior at the beginning of the simulation as seen in other simulations i.e., enhanced phase segregation near the polymer-vapor interface. (b)-(c) As the system evolves in time and solvent escapes the film, the polymer q forms more irregular structures near the interface. (d) Kinetic freezing encoded via the concentration dependent γ_i leads to a rougher film, which needs to be contrasted with the behavior of the previous simulation in Fig. 6, especially at $\hat{t} = 70000$ where, even though the solvent had been completely removed, the polymer p was able to diffuse from the smaller region of pure $\phi_p = 1$ on the left to the larger region on the right. Furthermore, pillar like morphology is obtained if the concentration dependence of γ_i is deliberately switched off (see Fig. S3 in the SI).

to the solvent evaporation. Although a number of choices can be made about γ_i for the dependence on the volume fraction, we chose a simple one, which leads to almost zero mobility for the solvent-free polymer blend. In particular, we take $\gamma_i \equiv \gamma_i(\boldsymbol{x},t) = \bar{\gamma}_i\phi_{\rm sl}(\boldsymbol{x},t)/\phi_i(\boldsymbol{x},t)$. This, in turn, leads to the polymer continuity equations implemented as

$$\dot{\phi}_i(\boldsymbol{x},t) - \nabla\cdot\left(\bar{\gamma}_i\phi_i(\boldsymbol{x},t)\phi_{\rm sl}(\boldsymbol{x},t)\nabla\left(\mu_i(\boldsymbol{x},t)+p(\boldsymbol{x},t)\right)\right) = 0 \quad i = {\rm p,q}. \tag{49}$$

and leads to $\dot{\phi}_i(\boldsymbol{x},t) \to 0$ for $\phi_{\rm sl}(\boldsymbol{x},t) \to 0$. Physically, this means that the polymer motion is kinetically frozen in place after the solvent has evaporated. Results of such a simulation run are shown in Fig. 7, which exhibit rougher interface formation between the polymer blend and the vapor phase. In these simulations, all the parameters are the same as in Table 1 except $\hat{\epsilon}_i^2 = 0.7$ and $\bar{\gamma}_i \equiv \gamma_i$ in the Table. Furthermore, we have used $\hat{\alpha}_p = -0.02$ and $\hat{\alpha}_q = 0.02$ for the surface energy terms. As earlier, reduction of $\hat{\epsilon}_i^2$ leads to more interfaces in the simulation (cf. Fig. 7). The effect of the concentration dependent mobility can be seen in Fig. 7, where a rougher film gets stabilized instead of pillars for the concentration indepedent mobility (also see Fig. S3 in the SI for comparisons with the simulation run without the effects of kinetic freezing).

Conclusions

We have developed a general methodology to model solvent evaporation in thin films. The methodology allows us to connect thermodynamics with the kinetics of phase separation and phase change in a consistent manner. In particular, rate of phase change (the source term, $S_{\rm sl}$) is shown to be directly coupled to the chemical potential of the liquid and the vapor, which is in qualitative agreement with a more general expression for the evaporative flux derived by Ward et al.[58] Using the self-consistent model developed in this work, we have studied the effects of the rate of phase change/reaction rate ($\hat{\lambda}$) and rate of escape of the vapor from the top boundary ($\omega_{\rm sv}$) on the motion of the interface. It is shown that not

only the velocity of the interface between the polymer blend and the vapor phase, but also the structure is determined self-consistently. For example, it is demonstrated that kinetic freezing resulting from concentration dependent mobility can lead to rougher films. Also, multiple vertical domains containing almost pure polymer in each of them can get stabilized due to the interplay of the square gradient energy coefficients and interactions with the substrates.

The methodology is general enough to include the effects of thermal gradients near the liquid-vapor interfaces although these were not included in the current work. Furthermore, coupling the continuity equations for the volume fractions to the microscopic equations of motion of the polymers[71] as well as electrostatics[72] should allow study of the underlying polymer dynamics and electrostatics, respectively, on the kinetics of phase separation in neutral and charged polymers.

Acknowledgements

This material is based upon work supported by the U.S. Department of Energy, Office of Science, Office of Workforce Development for Teachers and Scientists, Office of Science Graduate Student Research (SCGSR) program. The SCGSR program is administered by the Oak Ridge Institute for Science and Education for the DOE under contract number DE-AC05-06OR23100. This research was conducted at the Center for Nanophase Materials Sciences, which is a DOE Office of Science User Facility. RK acknowledges support from the Laboratory Directed Research and Development program at ORNL. SW was supported by a grant from the National Science Foundation (NSF-DMS 1418692). JL acknowledges support from National Science Foundation Grant NSF DMS-1719960, and P50GM76516 for the Center of Excellence in Systems Biology at the University of California, Irvine.

References

(1) de Gennes, P.-G.; Brochard-Wyart, F.; Quere, D. *Capillarity and Wetting Phenomena*; Springer Science + Business Media Inc., New York, 2004.

(2) Semenov, S.; Starov, V. M.; Velarde, M. G.; Rubio, R. G. Droplets evaporation: Problems and solutions. *The European Physical Journal Special Topics* **2011**, *197*, 265.

(3) Routh, A. F. Drying of thin colloidal films. *Reports on Progress in Physics* **2013**, *76*, 046603.

(4) Larson, R. G. Transport and deposition patterns in drying sessile droplets. *AIChE Journal* **2014**, *60*, 1538–1571.

(5) Larson, R. G. Twenty years of drying droplets. *Nature* **2017**, *550*, 466 EP –.

(6) Sellinger, A.; Weiss, P. M.; Nguyen, A.; Lu, Y.; Assink, R. A.; Gong, W.; Brinker, C. J. Continuous Self-assembly of organic-inorganic nanocomposite coatings that mimic nacre. *Nature* **1998**, *394*, 256–260.

(7) Kim, S.; Misner, M.; Xu, T.; Kimura, M.; Russell, T. Highly Oriented and Ordered Arrays from Block Copolymers via Solvent Evaporation. *Advanced Materials* **2004**, *16*, 226–231.

(8) Chang, J.-F.; Sun, B.; Breiby, D. W.; Nielsen, M. M.; Sölling, T. I.; Giles, M.; McCulloch, I.; Sirringhaus, H. Enhanced Mobility of Poly(3-hexylthiophene) Transistors by Spin-Coating from High-Boiling-Point Solvents. *Chemistry of Materials* **2004**, *16*, 4772–4776.

(9) Agar, J. C.; Damodaran, A. R.; Okatan, M. B.; Kacher, J.; Gammer, C.; Vasudevan, R. K.; Pandya, S.; Dedon, L. R.; Mangalam, R. V. K.; Velarde, G. A.; Jesse, S.; Balke, N.; Minor, A. M.; Kalinin, S. V.; Martin, L. W. Highly mobile ferroelastic domain

walls in compositionally graded ferroelectric thin films. *Nat Mater* **2016**, *15*, 549–556, Article.

(10) Shao, M.; Keum, J. K.; Kumar, R.; Chen, J.; Browning, J. F.; Das, S.; Chen, W.; Hou, J.; Do, C.; Littrell, K. C.; Rondinone, A.; Geohegan, D. B.; Sumpter, B. G.; Xiao, K. Understanding How Processing Additives Tune the Nanoscale Morphology of High Efficiency Organic Photovoltaic Blends: From Casting Solution to Spun-Cast Thin Film. *Advanced Functional Materials* **2014**, *24*, 6647–6657.

(11) Herath, N.; Das, S.; Zhu, J.; Kumar, R.; Chen, J.; Xiao, K.; Gu, G.; Browning, J. F.; Sumpter, B. G.; Ivanov, I. N.; Lauter, V. Unraveling the Fundamental Mechanisms of Solvent-Additive-Induced Optimization of Power Conversion Efficiencies in Organic Photovoltaic Devices. *ACS Applied Materials & Interfaces* **2016**, *8*, 20220–20229, PMID: 27403964.

(12) Onsager, L. Reciprocal Relations in Irreversible Processes. I. *Physical Review* **1931**, *37*, 405.

(13) Onsager, L. Reciprocal Relations in Irreversible Processes. II. *Physical Review* **1931**, *38*, 2265.

(14) Onsager, L. Theories and problems of liquid diffusion. *Annals of the New York Academy of Sciences* **1945**, *46*, 241–265.

(15) de Groot, S.; Mazur, P. *Non-equilibrium Thermodynamics*; Dover Books on Physics; Dover Publications, 1984.

(16) Doi, M.; Onuki, A. Dynamic coupling between stress and composition in polymer solutions and blends. *Journal de Physique II* **1992**, *2*, 1631–1656.

(17) Doi, M. Onsager's variational principle in soft matter. *Journal of Physics: Condensed Matter* **2011**, *23*, 284118.

(18) Doi, M. *Soft Matter Physics*; Oxford University Press, Oxford, 2013.

(19) Grmela, M.; Öttinger, H. C. Dynamics and thermodynamics of complex fluids. I. Development of a general formalism. *Phys. Rev. E* **1997**, *56*, 6620–6632.

(20) Ottinger, H. *Beyond Equilibrium Thermodynamics*; John Wiley and Sons, Inc.; John Wiley and Sons, Inc., 2005.

(21) Deegan, R. D.; Bakajin, O.; Dupon, T. F.; Huber, G.; Nagel, S. R.; Witten, T. A. Capillary flow as the cause of ring stains from dried liquid drops. *Nature* **1997**, *389*, 827.

(22) Deegan, R. D. Pattern formation in drying drops. *Phys. Rev. E* **2000**, *61*, 475–485.

(23) Deegan, R. D.; Bakajin, O.; Dupont, T. F.; Huber, G.; Nagel, S. R.; Witten, T. A. Contact line deposits in an evaporating drop. *Phys. Rev. E* **2000**, *62*, 756–765.

(24) Hu, H.; Larson, R. G. Evaporation of a Sessile Droplet on a Substrate. *The Journal of Physical Chemistry B* **2002**, *106*, 1334–1344.

(25) Bhardwaj, R.; Fang, X.; Attinger, D. Pattern formation during the evaporation of a colloidal nanoliter drop: a numerical and experimental study. *New Journal of Physics* **2009**, *11*, 075020.

(26) Bhardwaj, R.; Fang, X.; Somasundaran, P.; Attinger, D. Self-Assembly of Colloidal Particles from Evaporating Droplets: Role of DLVO Interactions and Proposition of a Phase Diagram. *Langmuir* **2010**, *26*, 7833–7842, PMID: 20337481.

(27) Ajaev, V. S. Spreading of thin volatile liquid droplets on uniformly heated surfaces. *Journal of Fluid Mechanics* **2005**, *528*, 279âĂŞ296.

(28) Teshigawara, R.; Onuki, A. Droplet evaporation in one-component fluids: Dynamic van der Waals theory. *EPL (Europhysics Letters)* **2008**, *84*, 36003.

(29) Onuki, A. Bubble and droplet motion in binary mixtures: Evaporation-condensation mechanism and Marangoni effect. *Phys. Rev. E* **2009**, *79*, 046311.

(30) Qian, T.; Wang, X.-P.; Sheng, P. A variational approach to moving contact line hydrodynamics. *Journal of Fluid Mechanics* **2006**, *564*, 333âĂŞ360.

(31) Qian, T.; Wu, C.; Lei, S. L.; Wang, X.-P.; Sheng, P. Modeling and simulations for molecular scale hydrodynamics of the moving contact line in immiscible two-phase flows. *Journal of Physics: Condensed Matter* **2009**, *21*, 464119.

(32) Klentzman, J.; Ajaev, V. S. The effect of evaporation on fingering instabilities. *Physics of Fluids* **2009**, *21*, 122101.

(33) Eggers, J.; Pismen, L. M. Nonlocal description of evaporating drops. *Physics of Fluids* **2010**, *22*, 112101.

(34) Maki, K. L.; Kumar, S. Fast Evaporation of Spreading Droplets of Colloidal Suspensions. *Langmuir* **2011**, *27*, 11347–11363, PMID: 21834573.

(35) Rednikov, A.; Colinet, P. Singularity-free description of moving contact lines for volatile liquids. *Phys. Rev. E* **2013**, *87*, 010401.

(36) Oron, A.; Davis, S. H.; Bankoff, S. G. Long-scale evolution of thin liquid films. *Rev. Mod. Phys.* **1997**, *69*, 931–980.

(37) Xu, X.; Thiele, U.; Qian, T. A Variational approach to thin film hydrodynamics of binary mixtures. *Journal of Physics: Condensed Matter* **2015**, *27*, 085005.

(38) Clarke, N. Toward a Model for Pattern Formation in Ultrathin-Film Binary Mixtures. *Macromolecules* **2005**, *38*, 6775–6778.

(39) Coveney, S.; Clarke, N. Pattern Formation in Polymer Blend Thin Films: Surface Roughening Couples to Phase Separation. *Phys. Rev. Lett.* **2014**, *113*, 218301.

(40) Thiele, U. Note on thin film equations for solutions and suspensions. *The European Physical Journal Special Topics* **2011**, *197*, 213.

(41) Thiele, U.; Todorova, D. V.; Lopez, H. Gradient Dynamics Description for Films of Mixtures and Suspensions: Dewetting Triggered by Coupled Film Height and Concentration Fluctuations. *Phys. Rev. Lett.* **2013**, *111*, 117801.

(42) Thiele, U. Patterned deposition at moving contact lines. *Advances in Colloid and Interface Science* **2014**, *206*, 399 – 413.

(43) Hohenberg, P. C.; Halperin, B. I. Theory of dynamic critical phenomena. *Rev. Mod. Phys.* **1977**, *49*, 435–479.

(44) de Gennes, P. Instabilities during the evaporation of a film: Non-glassy polymer + volatile solvent. *The European Physical Journal E* **2001**, *6*, 421–424.

(45) de Gennes, P. Solvent evaporation of spin cast films: "crust" effects. *The European Physical Journal E* **2002**, *7*, 31–34.

(46) Ozawa, K.; Okuzono, T.; Doi, M. Diffusion Process during Drying to Cause the Skin Formation in Polymer Solutions. *Japanese Journal of Applied Physics* **2006**, *45*, 8817.

(47) Okuzono, T.; Ozawa, K.; Doi, M. Simple Model of Skin Formation Caused by Solvent Evaporation in Polymer Solutions. *Phys. Rev. Lett.* **2006**, *97*, 136103.

(48) Wodo, O.; Ganapathysubramanian, B. Modeling morphology evolution during solvent-based fabrication of organic solar cells. *Computational Materials Science* **2012**, *55*, 113 – 126.

(49) Kouijzer, S.; Michels, J. J.; van den Berg, M.; Gevaerts, V. S.; Turbiez, M.; Wienk, M. M.; Janssen, R. A. J. Predicting Morphologies of Solution Processed Polymer:Fullerene Blends. *Journal of the American Chemical Society* **2013**, *135*, 12057–12067, PMID: 23863101.

(50) Paradiso, S. P.; Delaney, K. T.; García-Cervera, C. J.; Ceniceros, H. D.; Fredrickson, G. H. Block Copolymer Self Assembly during Rapid Solvent Evaporation: Insights into Cylinder Growth and Stability. *ACS Macro Letters* **2014**, *3*, 16–20.

(51) Wodo, O.; Ganapathysubramanian, B. How do evaporating thin films evolve? Unravelling phase-separation mechanisms during solvent-based fabrication of polymer blends. *Applied Physics Letters* **2014**, *105*, 153104.

(52) Paradiso, S. P.; Delaney, K. T.; GarcÃŋa-Cervera, C. J.; Ceniceros, H. D.; Fredrickson, G. H. Cyclic Solvent Annealing Improves Feature Orientation in Block Copolymer Thin Films. *Macromolecules* **2016**, *49*, 1743–1751.

(53) Chao, H.; Koski, J.; Riggleman, R. A. Solvent vapor annealing in block copolymer nanocomposite films: a dynamic mean field approach. *Soft Matter* **2017**, *13*, 239–249.

(54) Peter, S.; Meyer, H.; Baschnagel, J. Molecular dynamics simulations of concentrated polymer solutions in thin film geometry. II. Solvent evaporation near the glass transition. *The Journal of Chemical Physics* **2009**, *131*, 014903.

(55) Cheng, S.; Lechman, J. B.; Plimpton, S. J.; Grest, G. S. Evaporation of Lennard-Jones fluids. *The Journal of Chemical Physics* **2011**, *134*, 224704.

(56) Barrett, J.; Clement, C. Kinetic evaporation and condensation rates and their coefficients. *Journal of Colloid and Interface Science* **1992**, *150*, 352 – 364.

(57) Persad, A. H.; Ward, C. A. Expressions for the Evaporation and Condensation Coefficients in the Hertz-Knudsen Relation. *Chemical Reviews* **2016**, *116*, 7727–7767, PMID: 27314250.

(58) Ward, C. A.; Fang, G. Expression for predicting liquid evaporation flux: Statistical rate theory approach. *Phys. Rev. E* **1999**, *59*, 429–440.

(59) Ward, C. A. *Journal of Non-Equilibrium Thermodynamics*; 2002; Vol. 27; Chapter Liquid-Vapour Phase Change Rates and Interfacial Entropy Production, p 289, 3.

(60) Thiele, U.; Madruga, S.; Frastia, L. Decomposition driven interface evolution for layers of binary mixtures. I. Model derivation and stratified base states. *Physics of Fluids* **2007**, *19*, 122106.

(61) Cahn, J. W.; Hilliard, J. E. Free Energy of a Nonuniform System. I. Interfacial Free Energy. *The Journal of Chemical Physics* **1958**, *28*, 258–267.

(62) Bond, M.; Struchtrup, H. Mean evaporation and condensation coefficients based on energy dependent condensation probability. *Phys. Rev. E* **2004**, *70*, 061605.

(63) Kazemi, M. A.; Nobes, D. S.; Elliott, J. A. W. Experimental and Numerical Study of the Evaporation of Water at Low Pressures. *Langmuir* **2017**, *33*, 4578–4591, PMID: 28445057.

(64) Fischer, H. P.; Maass, P.; Dieterich, W. Novel Surface Modes in Spinodal Decomposition. *Phys. Rev. Lett.* **1997**, *79*, 893–896.

(65) Fischer, H. P.; Maass, P.; Dieterich, W. Diverging time and length scales of spinodal decomposition modes in thin films. *EPL (Europhysics Letters)* **1998**, *42*, 49.

(66) Fredrickson, G. H. *The Equilibrium Theory of Inhomogeneous Polymers*; Oxford University, New York, 2006.

(67) Puri, S.; Binder, K. Surface-directed spinodal decomposition in a thin-film geometry: A computer simulation. *Journal of Statistical Physics* **1994**, *77*, 145–172.

(68) Madruga, S.; Thiele, U. Decomposition driven interface evolution for layers of binary mixtures. II. Influence of convective transport on linear stability. *Physics of Fluids* **2009**, *21*, 062104.

(69) Bribesh, F. A. M.; Fraštia, Ľ.; Thiele, U. Decomposition driven interface evolution for layers of binary mixtures. III. Two-dimensional steady films with flat and modulated surfaces. *Physics of Fluids* **2012**, *24*, 062109.

(70) Bribesh, F. A. M.; Madruga, S. Free surface liquid films of binary mixtures. Two-dimensional steady structures at off-critical compositions. *Physics of Fluids* **2016**, *28*, 032108.

(71) Edwards, S. F.; Muthukumar, M. Brownian dynamics of polymer solutions. *Macromolecules* **1984**, *17*, 586–596.

(72) Kumar, R.; Mahalik, J. P.; Bocharova, V.; Stacy, E. W.; Gainaru, C.; Saito, T.; Gobet, M. P.; Greenbaum, S.; Sumpter, B. G.; Sokolov, A. P. A Rayleighian approach for modeling kinetics of ionic transport in polymeric media. *The Journal of Chemical Physics* **2017**, *146*, 064902.

For Table of Contents

Modeling solvent evaporation during thin film formation in phase separating polymer mixtures

John Cummings, John S. Lowengrub, Bobby G. Sumpter, Steven M. Wise, and Rajeev Kumar

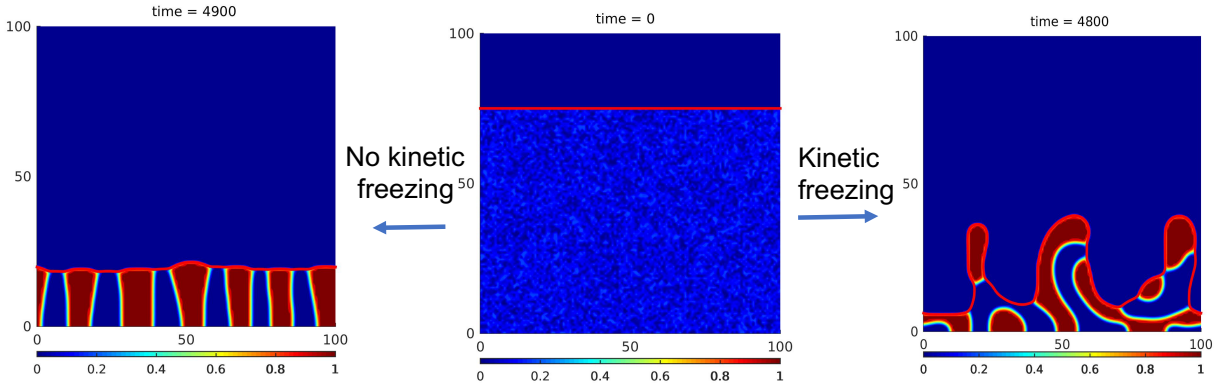

Figure 8: For the table of contents